AD-A190 281 AMPLIFICATION OF SIGNALS IN FIBER OPTICS USING THE STIMULATED RAMAN EFFECT(U) NAVAL OCEAN SYSTEMS CENTER SAN DIEGO CA S D RUSSELL ET AL. SEP 87 NOSC/TR-1196

1/1

UNCLASSIFIED

F/G 9/3

NL

END
DATE
FILMED
4 88

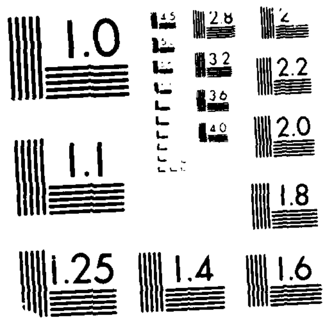

MICROCOPY RESOLUTION TEST CHART

[illegible]

NOSC TR 1196

AD-A190 281

NOSC

NAVAL OCEAN SYSTEMS CENTER San Diego, California 92152-5000

(4)

DTIC FILE COPY

NOSC TR 1196

Technical Report 1196
September 1987

Amplification of Signals in Fiber Optics Using the Stimulated Raman Effect

S. D. Russell
T. C. Stamnitz

UNITED STATES NAVY · NAVAL OCEAN SYSTEMS CENTER

Approved for public release; distribution is unlimited.

NAVAL OCEAN SYSTEMS CENTER

San Diego, California 92152-5000

E. G. SCHWEIZER, CAPT, USN
Commander

R. M. HILLYER
Technical Director

ADMINISTRATIVE INFORMATION

The work performed in this report was Phase 1 of an Independent Exploratory Development project funded by the Space and Naval Warfare Systems Command.

Released by
A. T. Nakagawa, Head
Advanced Fiber Optic
Systems Branch

Under authority of
D. K. Moore, Head
Advanced Systems
Division

ACKNOWLEDGEMENTS

The authors wish to thank Dr. H. E. Rast and the other members of Code 562 for the use of their facilities and their invaluable assistance throughout the course of this research; Dr. F. Hanson of Code 843 for the loan of equipment and consultation on the Nd:YAG laser system; Dr. G. Massey of San Diego State University for insight into the development of a pump laser; and Dr. C. T. Chang, also of San Diego State University, for providing the 5.5-km fiber used in these experiments.

PK

UNCLASSIFIED
SECURITY CLASSIFICATION OF THIS PAGE

REPORT DOCUMENTATION PAGE

1a REPORT SECURITY CLASSIFICATION UNCLASSIFIED	1b RESTRICTIVE MARKINGS
2a SECURITY CLASSIFICATION AUTHORITY	3 DISTRIBUTION AVAILABILITY OF REPORT Approved for public release; distribution is unlimited.
2b DECLASSIFICATION DOWNGRADING SCHEDULE	
4 PERFORMING ORGANIZATION REPORT NUMBER(S) NOSC TR 1196	5 MONITORING ORGANIZATION REPORT NUMBER(S)
6a NAME OF PERFORMING ORGANIZATION Naval Ocean Systems Center 6b OFFICE SYMBOL (if applicable) 534/562	7a NAME OF MONITORING ORGANIZATION
6c ADDRESS (City, State and ZIP Code) Advanced Fiber-Optic Systems Branch/ Optical Electronics Branch San Diego, CA 92152-5000	7b ADDRESS (City, State and ZIP Code)
8a NAME OF FUNDING SPONSORING ORGANIZATION Space and Naval Warfare Systems Command 8b OFFICE SYMBOL (if applicable)	9 PROCUREMENT INSTRUMENT IDENTIFICATION NUMBER
8c ADDRESS (City, State and ZIP Code) Washington, DC 20360	10 SOURCE OF FUNDING NUMBERS PROGRAM ELEMENT NO: 62936N PROJECT NO: RV36120 TASK NO: 534-ZE53 AGENCY ACCESSION NO:

11 TITLE (include Security Classification)

Amplification of Signals in Fiber Optics Using the Stimulated Raman Effect

12 PERSONAL AUTHOR(S)

S.D. Russell, T. Stamnitz

13a TYPE OF REPORT	13b TIME COVERED	14 DATE OF REPORT (Year, Month, Day)	15 PAGE COUNT
Interim	FROM Oct 1986 TO Apr 1987	September 1987	45

16 SUPPLEMENTARY NOTATION

17 COSATI CODES			18 SUBJECT TERMS (Continue on reverse if necessary and identify by block number)
FIELD	GROUP	SUB-GROUP	stimulated Raman scattering, optical-fiber transmission, photons, Stokes, anti-Stokes, pump wavelength

19 ABSTRACT (Continue on reverse if necessary and identify by block number)

This report details phase 1 of an Independent Exploratory Development project designed to investigate the feasibility of developing nonlinear optical transmission lines. The report gives a brief review of the theoretical basis and a description of the experimental design, prototype setup, and results. The appendices serve as a reference for future investigators.

20 DISTRIBUTION AVAILABILITY OF ABSTRACT ☐ UNCLASSIFIED/UNLIMITED ☒ SAME AS RPT ☐ DTIC USERS	21 ABSTRACT SECURITY CLASSIFICATION UNCLASSIFIED
22a NAME OF RESPONSIBLE INDIVIDUAL S.D. Russell	22b TELEPHONE (include Area Code) 619-225-6221 22c OFFICE SYMBOL Code 553

DD FORM 1473, 84 JAN

83 APR EDITION MAY BE USED UNTIL EXHAUSTED
ALL OTHER EDITIONS ARE OBSOLETE

UNCLASSIFIED
SECURITY CLASSIFICATION OF THIS PAGE

DD FORM 1473, 84 JAN

SUMMARY

OBJECTIVE

The feasibility of using stimulated Raman scattering (SRS) to obtain increased unrepeatered distances in undersea, long-haul optical-fiber transmission was demonstrated.

RESULTS

Phase 1 resulted in the generation of new wavelengths in the Raman fiber laser and the amplification of spontaneously scattered light at two wavelengths (1.117 μm and 1.18 μm).

FUTURE PLANS

The next milestone in the development of a viable amplification system is the generation of the third through fifth Stokes lines which should be attainable by further depletion of the pump beam (Phase 2). Extension to long-haul experiments can then be initiated.

CONTENTS

ILLUSTRATIONS

TABLES

APPENDICES

ILLUSTRATIONS

TABLES

LIST OF SYMBOLS AND ABBREVIATIONS

α	Linear loss coefficient
Δ	Fiber core-cladding index difference (%)
ϵ	Relative permittivity or dielectric constant
λ	Wavelength
λ_s	Stokes wavelength
σ	Spontaneous Raman cross-section
$\omega_i, \omega_s, \omega_p$	Idler, signal and pump frequencies
ω_I, ω_S	Incident and scattered photon frequencies
Ω	Phonon frequency (GHz) or phonon wavenumber (cm^{-1})
Δn	Refractive index dispersion
Δt	Temporal dispersion
π	Pi (3.14159...)
h	Planck's constant (6.626×10^{-34} J s)
h	Planck's constant/2π (1.055×10^{-34} J s)
ϕ	Phase
Ge	Germanium
SiO_2	Silicon dioxide
$LiNbO_3$	Lithium niobate
$LiIO_3$	Lithium iodate
KDP	Potassium dihydrogen phosphate ($H_2K_2PO_4$)
BBO	Beta barium borate (β-$BaBO_3$)
$\|i\rangle, \|f\rangle$	Initial and final state
BS	Beam splitter
c	Velocity of light
DP	Dispersing prism or monochrometer
FWHM	Full width at half maximum amplitude
g	Raman gain coefficient
HR	High reflector
HV	High Voltage
I_{po}	Effective input pump intensity
IR	Infrared
ℓ	Actual fiber length
L	Cavity length

L_{eff}	Effective gain length
L_{opt}	Optimum interaction length
L#	Lens number
LPS	Laser Power Supply
LT	Laser Transmitter
M#	Mirror number
n	Bose-Einstein thermal population factor
NBF	Narrow band filter
NDF	Neutral density filter
n_i, n_s, n_p	Refractive index at idler, signal, and pump λ's
OC	Output coupler
OD	Outer diameter or overall diameter
OPG	Optical parametric generation
OPO	Optical parametric oscillator
P_s	Output signal power
P_{so}	Input signal power
P_{th}	SRS threshold power density
PFN	Pulse-forming network
r_{OC}, r_{HR}	Radius of curvature of output coupler and high reflector
R,%R	Percent reflectivity (usually at 1.064 μm)
Rep Rate	Repetition rate (Hz)
S#	Stokes line number
SHG	Second harmonic generation
SM	Single mode
SRS	Stimulated Raman scattering
V_c	PFN Capacitor voltage
V_{max}, V_{min}	Maximum and minimum laser operating voltage measured at the PFN capacitor

1.0 INTRODUCTION

1.1 OBJECTIVE

The objective of this project is to demonstrate the feasibility of using stimulated Raman scattering (SRS) to obtain increased unrepeatered distances in undersea, long-haul optical fiber transmission (200-300 km).

1.2 MOTIVATION

Long-haul undersea optical-fiber telemetry links require regenerators to amplify the attenuated signals after distances on the order of 75 km. The reliability and cost of a long-haul communication link could be improved by eliminating the optical regenerators even while using more complex terminal equipment. This is due to the difficulty and costs involved in retrieval and repair operations, in addition to the initial costs of the hermetically sealed regenerators.

1.3 APPROACH

The approach to this project is divided into two phases. Phase 1 requires the observation of Raman gain in a short (less than 10-km) optical fiber. This involves using available resources to set up a prototype SRS experiment and documenting the procedures and results pertinent to Naval applications. Phase 2 requires the optimization of experimental technique and the demonstration of Raman gain in long-haul transmission. This report covers phase 1 of this project.

2.0 REVIEW OF STIMULATED RAMAN SCATTERING

2.1 LIGHT SCATTERING BASICS

The theory of light scattering by solids has been reviewed by several authors. Reference 1 is one example. The theory generally results in a two-photon process (figure 1) which is described by an incident photon of energy $h\omega_I$ interacting with the solid in its initial state $|i>$ which may include some elementary excitation with energy $h\Omega$. (In our applications the excitation is a phonon.) After the interaction, the solid is in a final state $|f>$ and a scattered photon is created with energy $h\omega_S$ where

$$h\omega_S = h\omega_I +/- h\Omega \quad (1)$$

The two cases represented by equation (1) have historically been named Stokes and anti-Stokes processes corresponding to the scattered photon having less energy or more energy than the initial photon, respectively. If no photons of frequency ω_S exist in the initial state $|i>$, the scattering process is called spontaneous Raman scattering. If there are photons of frequency ω_S present in the initial state, the process is called stimulated Raman scattering (SRS).

SRS can therefore be generated if the intensity of the incident beam of photons is sufficiently large such that there is coupling between the Stokes wave and the phonon resulting in enhanced scattering by the incoming photons (references 2,3). In this situation, the electric susceptibility, which describes the response of the solid to the electric field of the incident photons, must include nonlinear terms. Optical-fibers represent an ideal solid for this type of interaction due to their small cross-sectional area (resulting in high power density) and long interaction length. SRS leads to the two nonlinear effects described below which are important for optical-fiber communications: wavelength conversion and Stokes gain.

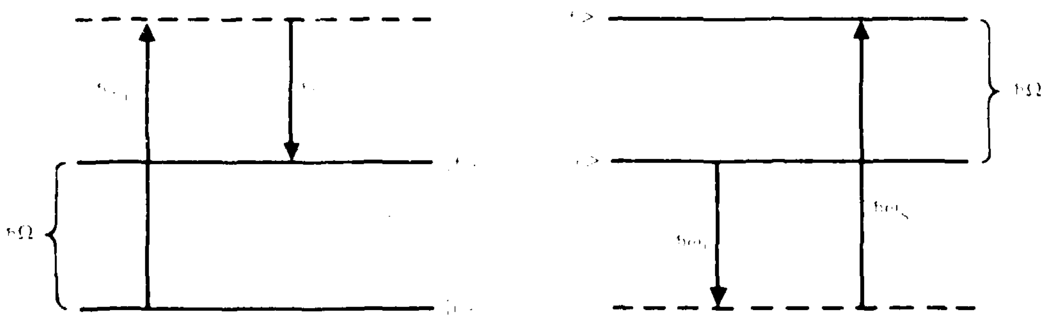

Figure 1 Two-photon scattering processes

2.2 SRS FEATURES

Wavelength conversion is a process in which the incident (pump) wavelength gets shifted to a new wavelength through the creation of phonons of energy $h\Omega$ (where Ω is the phonon frequency) while simultaneously depleting the pump wavelength. The wavelength of the newly created photons (called the Stokes wave or line) is determined by equation (1). At sufficiently high intensities, this effect can cascade, resulting in the generation of many new wavelengths due to the newly generated Stokes line acting as a pump for the subsequent Stokes line. Figure 2 shows the creation of new wavelengths (after Cohen and Lin, in reference 4) from intense pumping of 1.06 μm light into SiO_2 fiber. The generation of the first five Stokes lines (labeled S_1 through S_5) is shown, with a separation of approximately 490 cm^{-1} between the lines which corresponds to the wave number of the phonon created in this process. Selection and generation of new wavelengths in the near-infrared (IR) is, therefore, possible with intense pumping of a fiber with suitable phonon frequency.

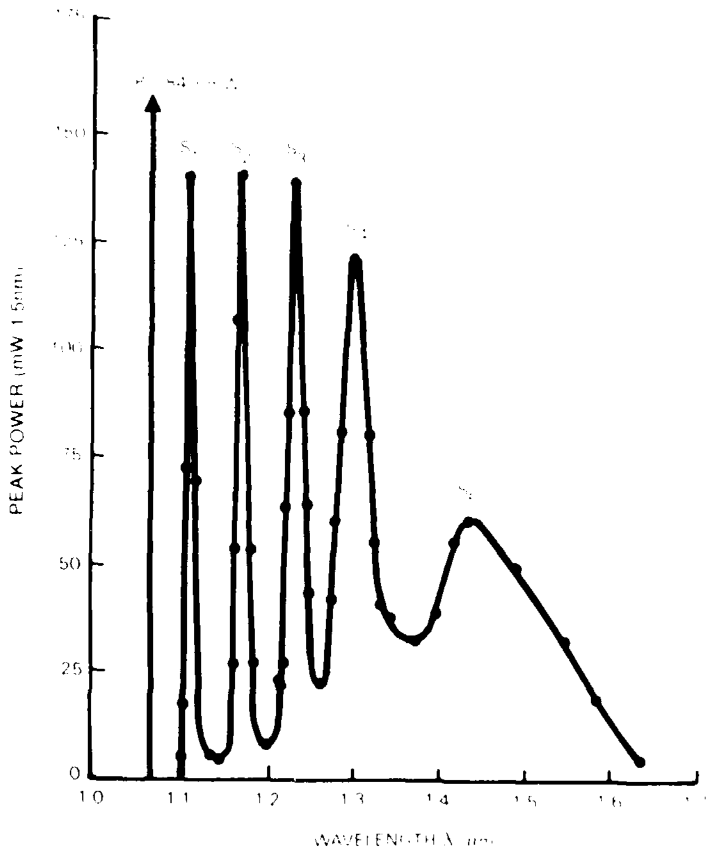

Figure 2. Generation of five orders of Stokes wavelengths from Cohen and Lin (reference 4)

The design of a Raman amplifier is based on the second SRS feature, the observation of Stokes gain in optical fibers. The amplification can be described by the formula

$$P_s/P_{so} = \exp\,(gI_{po}L_{eff}) \;, \tag{2}$$

where P_s/P_{so} is the ratio of the output signal power to the input signal power, I_{po} is the effective input pump intensity, L_{eff} is the effective gain length and g is the Raman gain coefficient (references 5, 6). For a given fiber length and pump intensity, the amplification is determined by the Raman gain coefficient which is related to the spontaneous Raman cross section (σ) by the equation,

$$g = \frac{\sigma\lambda_s^3}{c^2h\epsilon(n+1)} \tag{3}$$

where λ_s is the Stokes wavelength, c is the velocity of light, h is Planck's constant, ϵ is the dielectric constant at λ_s, and n is the Bose-Einstein thermal population factor. Equation 3 implies that optimum gain can be obtained by proper choice of material; for example, figure 3, which shows Raman gain curves for three representative glasses (reference 7). The chosen material should have the largest Raman gain coefficient at the desired wavenumber of the generated Stokes line.

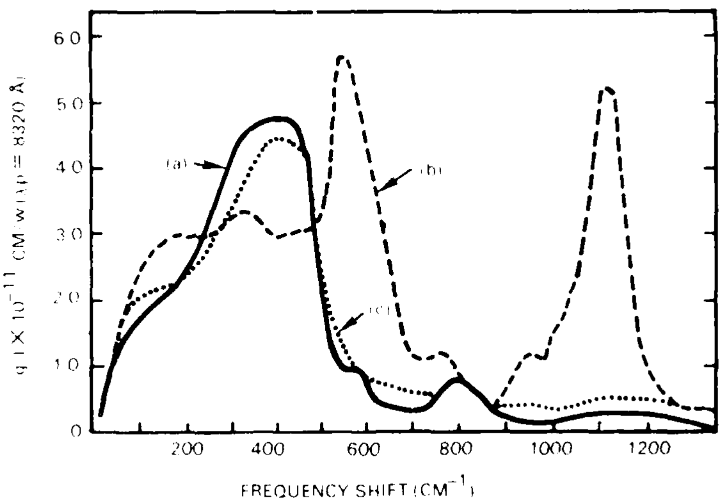

Figure 3. Raman gain curves for three representative glasses: (a) Fused quartz, (b) Soda-lime silicate (20:10:70), and (c) Pyrex (reference 7).

3.0 EXPERIMENTAL DESIGN

3.1 THE RAMAN AMPLIFIER

Using the above mentioned features one can design a Raman amplifier utilizing SRS in an optical-fiber. Figure 4 shows schematically the generic setup, where both the signal and pump beams are simultaneously launched into an optical-fiber (or optical-transmission line). At the output of the fiber the signal beam has been amplified (according to equation 2) and can be separated from the pump beam for subsequent signal processing.

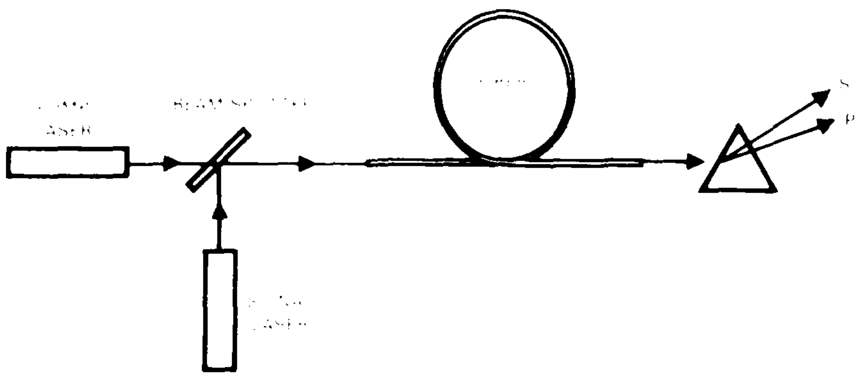

Figure 4 The Raman amplifier

3.2 FIBER REQUIREMENTS

Since the signal amplification is directly related to the Raman gain coefficient (g), it is desirable to use a glass fiber with the largest g value. Generally, choice of fiber composition is based on bandwidth, cutoff wavelength, attenuation, strength, and cost requirements (to name a few) and not on its nonlinear properties. In the near future, it is not likely to change since the capability of tailoring the fiber core composition is not yet perfected. Therefore, one must optimize the fiber using the two available parameters, length and core diameter.

The effective input pump power (I_{po} in equation 2) is determined from the guide-mode intensity profile. The following assumes a Gaussian beam profile (TEM_{oo}),

$$I_{po} = \frac{P_{po}}{\pi r^2} \tag{4}$$

where P_{po} is the peak input pump power, and r is the 1/e intensity radius. Therefore, a smaller beam radius yields higher effective pump power and greater amplification. This implies that the use of single-mode fibers, which typically have core diameters between 4 to 10 μm, are better suited for Raman amplification (compared to multimode fibers with 50 to 100-μm diameter core).

The fiber length is also an important parameter, since there must be sufficient interaction length for the pump and signal beams. Also, all fibers have linear losses (represented by their *linear attenuation coefficient* α); thus, the effective gain length (L_{eff} in equation 2) is less than the actual length (ℓ) by

$$L_{eff} = [1- \exp(-\alpha\ell]/\alpha. \qquad (5)$$

For optimum interaction, the pump beam should be entirely converted into the Stokes *line when* L_{eff} - $1/\alpha$. *Table 1 shows the optimum interaction length* L_{opt} *for various* fiber attenuations (in cm^{-1}) and losses (in dB/km).

Table 1. Optimum interaction length for various fiber attenuations.

Loss (dB/km)	α (cm^{-1})	L_{opt} (km)
0.2	4.6×10^{-7}	21.6
0.4	9.2×10^{-7}	10.8
0.6	1.4×10^{-6}	7.2
0.8	1.8×10^{-6}	5.4
1.0	2.3×10^{-6}	4.3
2.0	4.6×10^{-6}	2.1
3.0	6.9×10^{-6}	1.4
4.0	9.2×10^{-6}	1.1
5.0	1.2×10^{-5}	0.9

3.3 PUMP REQUIREMENTS

The pump wavelength must be one (or an integral number) of Stokes lines away from the signal wavelength so that pump depletion will amplify the signal wavelength. Since the signal wavelength for fiber communication must suffer minimum spectral dispersion (1.3 μm typically) or minimum attenuation (1.55 μm), one can calculate the required pump wavelength by assuming a Stokes' shift of 469 cm^{-1} for SiO_2 core fiber (reference 9). The required wavelength is calculated by transforming the pump wavelength to wavenumber units and adding the Stokes shift, then one obtains 6500 cm^{-1} + 469 cm^{-1}. This corresponds to a wavelength of 1.43 μm required for the pump. Similarly, a pump wavelength of 1.22 μm is calculated to amplify a signal at 1.3 μm.

An estimate of the threshold power density to generate SRS is given by (*references 10, 11*)

$$P_{th}\ [W/cm^2] \approx 20\alpha/g \qquad (6)$$

with α in units of cm^{-1} and g in cm/W. Using a value of $g = 4.5 \times 10^{-11}$ cm/W from figure 3 for fused quartz, and a range of fiber attenuations from 0.4-5.0 dB/km, the power density required to generate SRS is between 0.2-2.6 MW/cm^2, respectively.

3.4 GENERATION OF THE PUMP WAVELENGTH

Methods of generating the pump wavelength with sufficient power to generate SRS were sought. Several sources of coherent radiation could be ruled out due to their low-output power levels in the desired near-IR range (1.2-1.4 μm), namely gas and solid-state lasers. Among these, semiconductor laser arrays and color-center lasers seem most promising for generation of high-power near-IR radiation but are not yet available. Transitions in gas lasers in the near-IR are weak, and require low operating pressures. This would lead to stability and impurity problems impractical for systems applications. Dye lasers offer further limitations with the unavailability of any near-IR dye. On this basis, the generation of near-IR wavelengths using a high power Nd:YAG as a primary pump were investigated. Two potentially viable alternatives were found; namely, optical parametric generation (OPG) and the Raman fiber laser.

OPG occurs when high intensity light (at the pump frequency ω_p) traverses a nonlinear crystal producing two scattered frequencies denoted by ω_s (the signal beam) and ω_i (the idler beam) under the phase-matching condition (reference 12):

$$\omega_p/n_p = \omega_s/n_s + \omega_i/n_i. \tag{7}$$

The refractive indices n_p, n_s, and n_i are the indices of the crystal at the corresponding frequency. The choice of frequencies is controlled by the tuning of the index via changes in temperature (for crystals such as $LiNbO_3$, KDP and its isomorphs) or angle (e.g. $LiIO_3$, BBO). Using a Nd:YAG laser as the primary pump at 1.064 μm to generate the secondary pump beam at 1.22 μm or 1.43 μm would result in the generation of the idler beam at 8.3 μm (or 4.2 μm respectively) from energy conservation considerations. These idler wavelengths lie in the absorption band for the available nonlinear crystals (see, for example, figure 5 for $LiIO_3$) thus making OPG impossible.

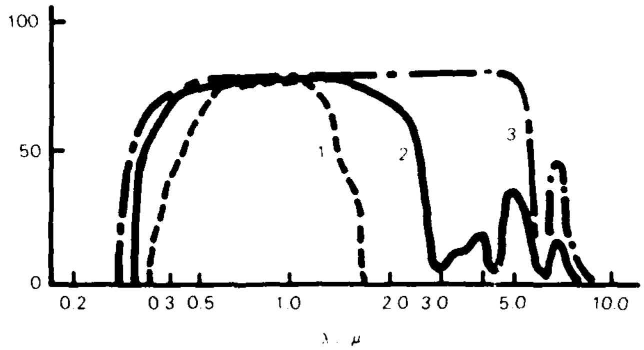

Figure 5. Transparency region in $LiIO_3$ (curve 2) from Izrailenko et. al. (reference 13).

The following two-step optical parametric generation is required: (1) second harmonic generation (SHG) to 0.532 μm which represents the degenerate case of equation 7 where $\omega_s = \omega_i$, and (2) generation of the 1.22 μm (or 1.43 μm) signal beam using the 0.532 μm light as the pump. Using the doubled Nd:YAG beam as the pump would result in the idler wavelength at 0.94 μm (or 0.85 μm respectively) which is in the transparent region of these crystals. The schematic of this two-step process to generate the pump for the Raman amplifier is shown in figure 6. The use of the

singly resonant optical parametric oscillator (OPO) to selectively amplify the signal beam in the cavity (formed by M1 and M2 in figure 6) has been shown (references 14, 15) to improve conversion efficiencies; however, typically less than 10-percent conversion is achieved away from degeneracy. Due to the moderate efficiencies (30-50 percent) in doubling the Nd:YAG, there is a requirement for extremely high intensity pulses from the primary pump source. While the intensities required to drive this two-stage setup are attainable with a Q-switched laser, the damage threshold of the nonlinear crystals is the limiting constraint. Current research into high damage threshold (~5 GW/cm_2 at 10 ns pulses) crystals such as BBO (reference 16) is being conducted, however, conversion efficiencies have not yet been obtained. Therefore, OPG was not considered the preferred method of generating the near-IR pump due to its limited conversion efficiencies and damage thresholds. It deserves, however, some consideration based on recent advances in BBO technology.

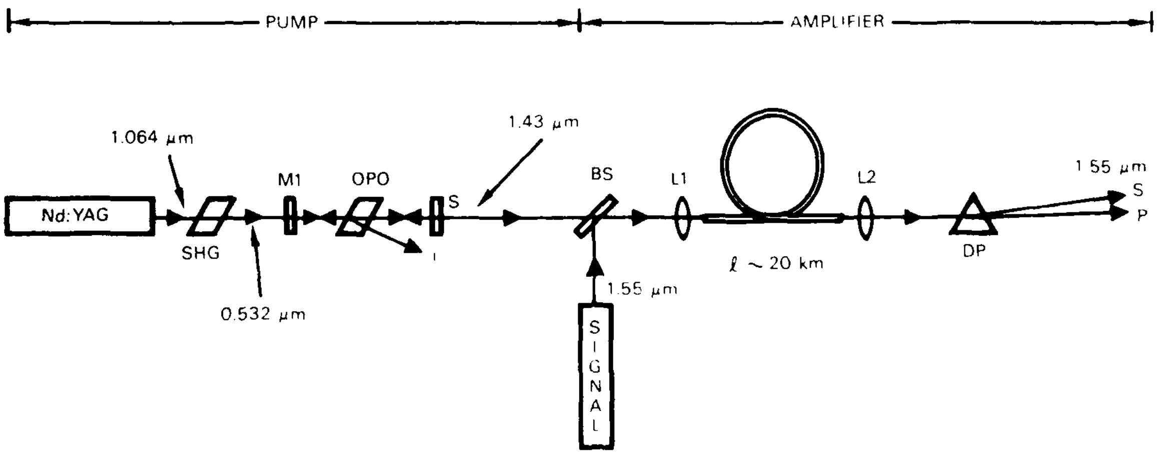

Figure 6. Raman amplifier with two-step OPG pump.

Figure 7 schematically illustrates the Raman amplifier using a Raman fiber–laser pump. The fiber laser utilizes the wavelength conversion and Stokes gain described earlier and is essentially identical to the Raman amplifier except for two features: (1) the output is generated from spontaneously generated Stokes light, therefore, input of a "signal" beam is not required, and (2) a resonating cavity can be inserted to improve conversion efficiency, effectively increasing the interaction length in this multipass mode. The major advantage of this technique over OPG is the observation of gain (reference 8) after a single pass through the fiber; consequently, this method of generating the amplifier pump was chosen for our research efforts. Using a Nd:YAG laser at 1.064 μm as the primary pump, the generation of the 1.22 μm (or 1.45 μm) pump beam for the amplifier can be obtained by filtering the output for the third or fifth Stokes line, respectively, in the SiO_2-core fiber.

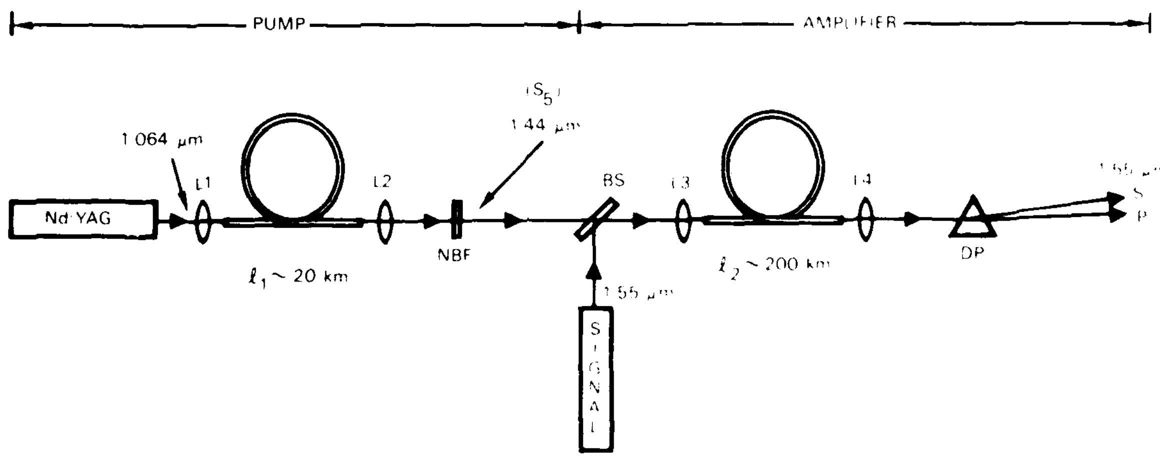

Figure 7. Raman amplifier with Raman fiber-laser pump

4.0 PROGRESS REPORT

4.1 PREFACE

Early research involved not only theoretical design of the experiment but also significant ground work in setting up a facility for nonlinear optics research. The primary pump laser was obtained on indefinite loan, however it required refurbishing of the laser head, transmitter, and cooling system as well as replacement of the Q-switch electronics and all of the optical components. The 3-phase, 208–V, 400–Hz, 20 A power line necessary for its operation required nearly six weeks for installation by the Public Works Center (PWC). Significant time was also invested in the specification and procurement of supplies (see Appendix B) necessary to implement the experiment outlined in this document.

4.2 CHARACTERIZING AND OPTIMIZING THE PRIMARY PUMP

Figure 8 shows a schematic of the refurbished Nd:YAG laser system used as the primary pump. The basic system is a militarized version of the GTE model 618 laser containing four major components: the power supply, transmitter, cooler, and cavity. The laser cavity which consists of the Nd:YAG rod, flashlamp, dual confocal mirrors, and cooling housing contained in the head together with the associated optics, was removed from the transmitter and mounted on an optical breadboard. This provided for (1) ease in adjustments and alignments with other optical components, (2) safe working distance from the high voltage pulse forming network (PFN) and Q-switch components in the transmitter, and (3) larger cavity length. The latter results in increased modal volume in the rod, thereby increasing laser gain (reference 17). Both the laser head and transmitter were cooled using a closed-cycle deionized water/air heat exchanger (denoted by dashed lines in figure 8 with associated flow arrows). The power supply provided the operating voltages for the cooler, transmitter, and head, and acted as the control center for generating laser pulses. Details on the system components are found in Appendix A.

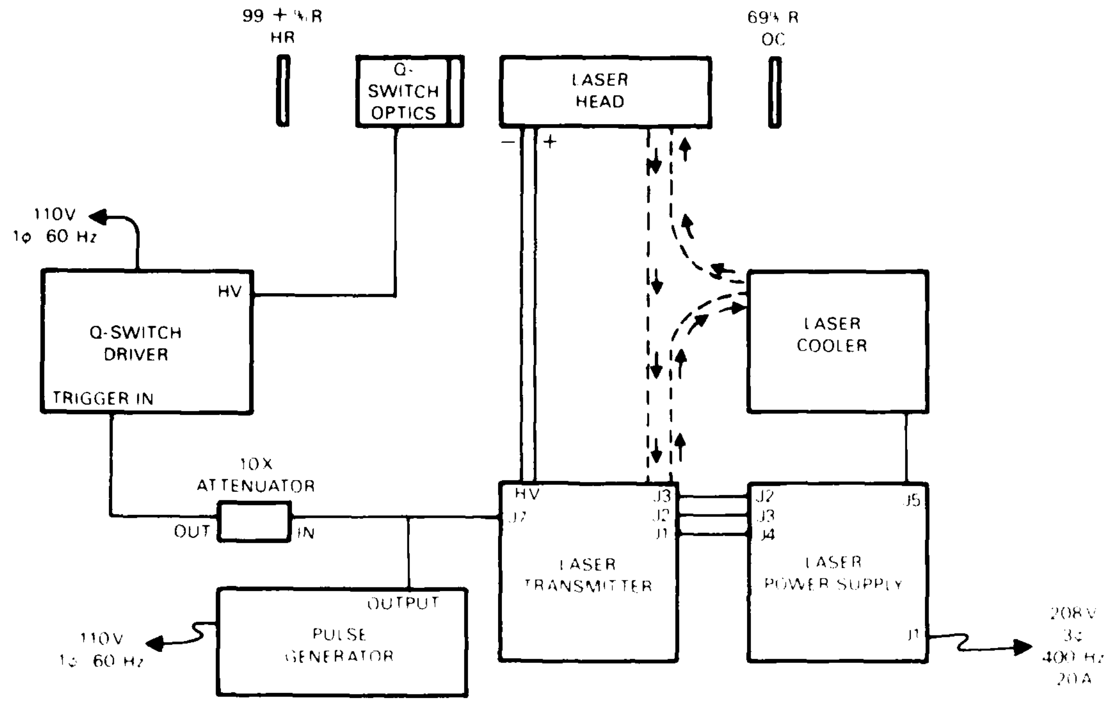

Figure 8 Refurbished Nd:YAG laser.

Optimal resonator design was determined empirically by measuring the output of the un-Q-switched laser (i.e., Q-switch optics removed from cavity). This involved the geometric configuration of the mirrors with respect to each other and the laser rod, and the selection of the mirrors. A hemispherical cavity was chosen which, furthermore, satisfied the stability condition,

$$0 < \left(1 - \frac{L}{r_{HR}}\right)\left(1 - \frac{L}{r_{OC}}\right) < 1 \qquad (8)$$

where "L' is the cavity length, and the radius of curvature of the high reflector (HR) and output coupler (OC) are given by r_{HR} and r_{OC}, respectively. A cavity length of 61 $\pm$ 1 cm resulted in maximum output in the TEM_{oo} mode with r_{OC}= 1.47 m and r_{HR}={inf}. Increasing cavity length to increase mode volume in the rod resulted in a higher-order mode structure; apparently, resulting from defects in the laser rod. Suppression of these higher-order modes was aided by placing the rod within 13 cm of the OC, thereby acting as the limiting aperture (0.635 cm diameter).

Figure 9 shows the laser output per pulse as a function of the OC reflectivity. Measurements were obtained using a Gentec Model #PRJ-D detector with Model #ED-500 calibrated head. In these measurements, the OC radius of curvature, cavity length, and HR were identical. The upper curve (open circles) represents the output at the maximum operating voltage ($V_{max} \equiv V_c$ = 420 V) and a repetition rate of 2 Hz. V_c is the voltage applied to the 100 μf PFN capacitor which fires the flashlamp. The

lower curve (closed circles) is the output at the minimum operating voltage ($V_{min} \equiv V_c = 333$ V). The maximum output occurred with the 69 percent R OC installed. Energies of approximately 275 mJ per pulse were obtained with this configuration.

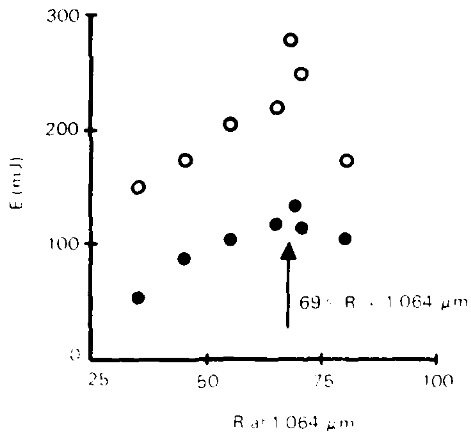

Figure 9. Laser output vs. OC reflectivity.

Figure 10 shows the un-Q-switched laser output power per pulse at 2 Hz as a function of the pulse forming network (PFN) capacitor voltage (and flash-lamp energy). The numerical value besides each data point are the nominal values of the voltage on the laser power-supply front panel (in arbitrary units). The expected linear relationship between the flashlamp energy and laser output is observed, with an overall efficiency of approximately 3 percent. Increased efficiency could be obtained by modifications to the rod/flashlamp housing to minimize flashlamp light loss through the secondary rod support, but was determined to be unnecessary in view of the laser's adequate output performance.

Significant performance degradation was observed with increased rep rate. This is demonstrated by figure 11 which shows the un-Q-switched laser output power per pulse at V_{min} as a function of rep rate. There is a large drop off above -25 Hz which is due to the large time constant involved in recharging the PFN capacitor. Above V_c .342 V (V = 5 in front panel units), the laser will not operate at rep rates $\geq$ 20 Hz. At 2 Hz, the laser shows unexplained optimal performance at all voltages. This is reproducible and may be attributable to flash-lamp performance.

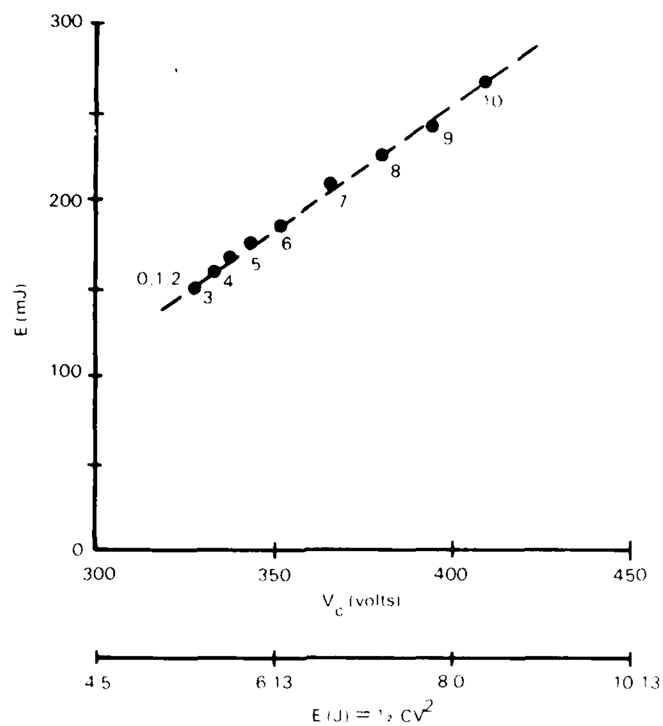

Figure 10. Laser output vs flashlamp energy.

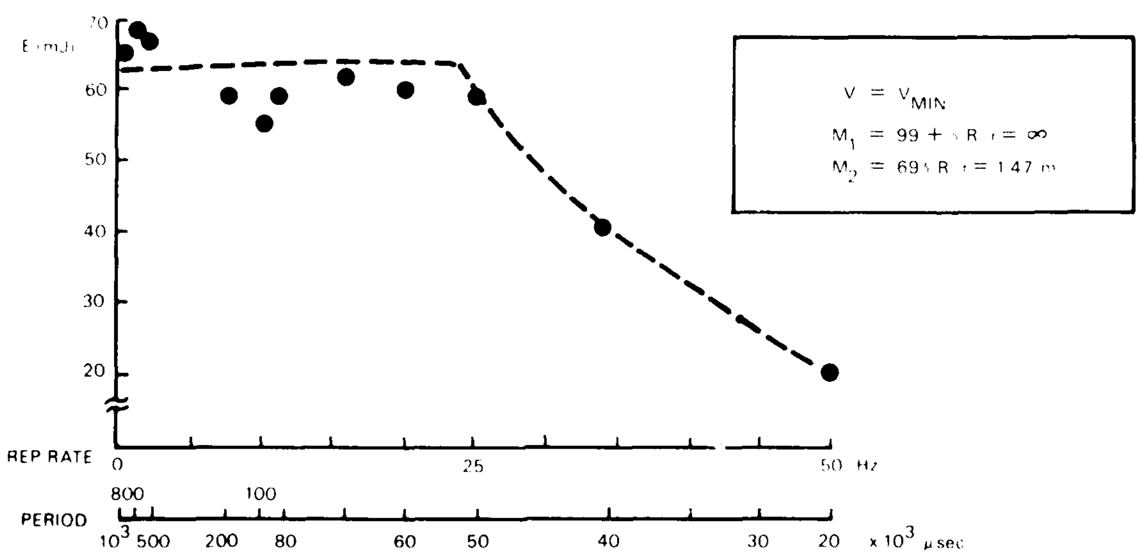

Figure 11. Laser output vs rep rate.

Installation of the Q-switch optics into the cavity results in an increase in losses by -60 percent, due primarily to surface reflections of the multi-element unit. Proper triggering of the pockels cell (Appendix A) produces a Q-switched pulse with FWHM -20 ns (figure 12) and a beam diameter of 6 mm measured using an Antel Model #AR-G10 Ge p-i-n photodiode. A summary of the optimized Nd:YAG laser performance is shown in table 2. Note that the peak powers listed in Table 2 are more than sufficient to generate SRS in single mode optical fibers assuming typical coupling efficiencies.

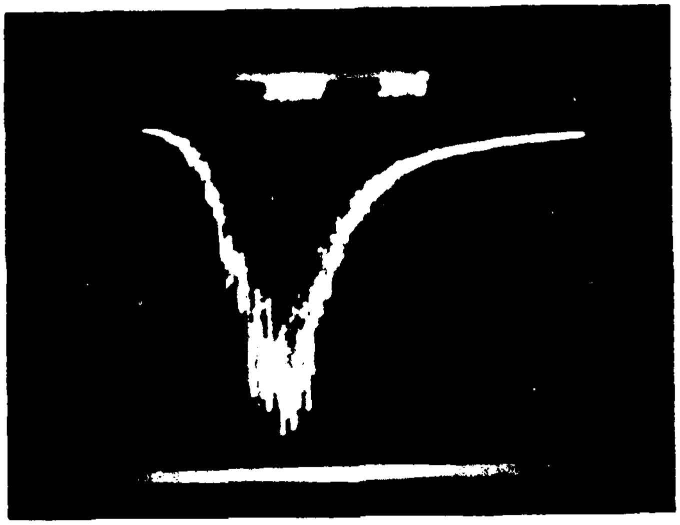

Figure 12. Q-switched Nd:YAG pulse.

Table 2. Nd:YAG laser performance summary.

Rep Rate (Hz)	V_c (Volts)	un-Q-sw E(mJ)	Q-sw E(mJ)	FWHM (nsec)	Peak power (MW)
1	328	47$\pm$1	34$\pm$1	20	1.42
1	342	54$\pm$1	38$\pm$1	20	1.58
1	410	97$\pm$1	64$\pm$1	20	2.67
2	328	54$\pm$1	39$\pm$1	20	1.63
2	342	64$\pm$1	46$\pm$1	20	1.92
2	410	106$\pm$1	68$\pm$1	20	2.83
10	328	35$\pm$1	25$\pm$1	20	1.04
10	342	48$\pm$1	34$\pm$1	20	1.42
10	410	75$\pm$1	45$\pm$1	20	1.88
20	328	24$\pm$1	19$\pm$1	20	0.79
20	342	34$\pm$1	24$\pm$1	20	1.00
20	410	----	----	--	----

4.3 AMPLIFICATION IN 5.5-KM LENGTH OF SINGLE-MODE FIBER

Figure 13(a) shows the single pass Raman fiber laser used to obtain wavelength conversion and Stokes gain in a 5.5-km length of single-mode fiber (for fiber specifications see Appendix C). The primary pump consisted of the refurbished Nd:YAG laser, operating typically at 10 Hz (Q-switched to 20 ns FWHM). However, Stokes lines were observed throughout the operating range 1 Hz to 20 Hz. The lenses (L1, L2) used to launch light into and out of the fiber (figure 13(b)) are critical for coupling efficiency. Use of microscope objectives usually antireflection (AR) coated for the visible, resulted in 6 percent losses per objective. Upon the insertion of a diode laser focusing lens (AR coated for the 0.85 μm to 1.3 μm region), losses of -1 percent per lens were obtained.

Launching the light into the fiber required the following of a careful procedure to eliminate damage to the fiber end. The input end of the fiber was located approximately twice the focal distance from the lens, and roughly aligned by viewing the cladding modes with an IR viewer. Output could then be detected from the fiber using the Ge detector described earlier. Transverse alignment of the fiber ends was performed by maximizing the detected signal. The light from the fiber output was focused onto the detector with lens (L3) being attenuated by a neutral density filter (NDF) to prevent detector saturation. The input fiber end was then slowly translated toward the focal point of the lens. This gradually increased the amount of the pump beam launched into the fiber by increasingly filling the numerical aperture of the fiber until the threshold for Stokes generation was observed. Increasing the laser output by increasing V_c (figure 10 and corresponding text) also generated Stokes amplification.

Figure 14 shows the oscilloscope trace from the Ge detector at the fiber output exhibiting SRS. The sequence of photos (a) through (c) shows the gradual increase in filling the numeric aperture of the fiber. Figure 14 (a) shows only the pump beam, when the input power density was below the threshold required to generate SRS. Figure 14(b) shows both the pump beam and the first Stokes line (S1), whereas figure 14(c) shows at least one additional line (S1, S2, and possibly S3). Further increase in input power resulted in damage to the fiber end. Measuring the wavelengths of these lines was done by passing the fiber output through a Jarrell-Ash Model #82-020, 0.5 m Ebert scanning spectrometer with a 590 grooves/mm diffraction grating. Using slits of 200 μm (-1 nm resolution), the output showed three lines: 1.063 μm corresponding to the Nd:YAG pump, 1.117 μm corresponding to the first Stokes line in SiO_2 (with Ω = 469 cm^{-1}), and 1.18 μm corresponding to the second Stokes line in SiO_2. No evidence of the third Stokes line could be detected through the monochrometer.

Figure 13(a). Single-pass Raman fiber laser.

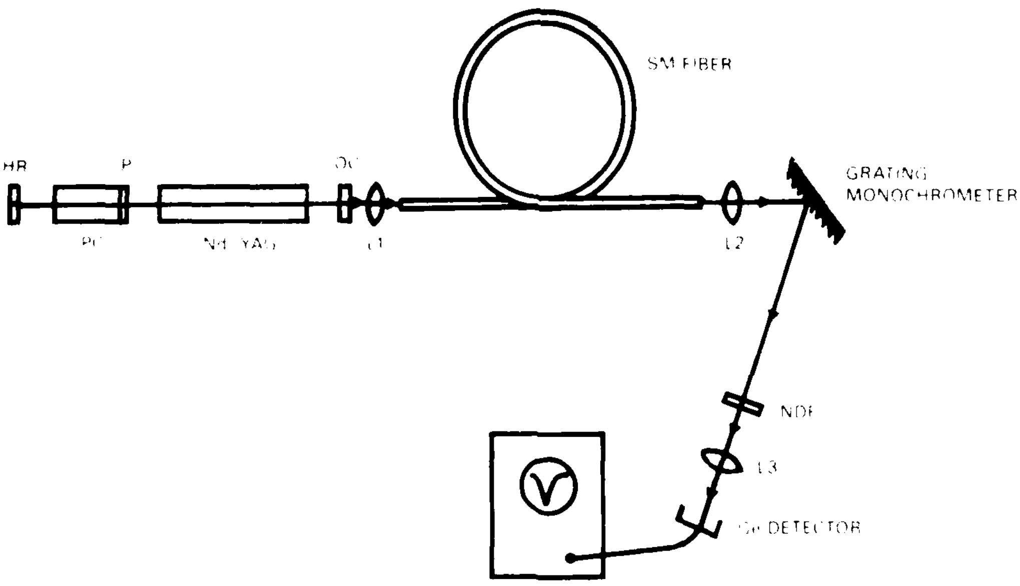

Figure 13(b). Fiber-laser schematic.

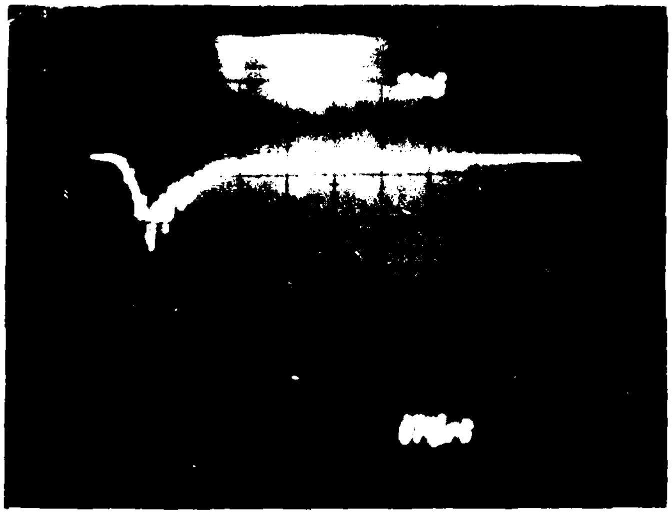

(a) Pump beam below SRS threshold

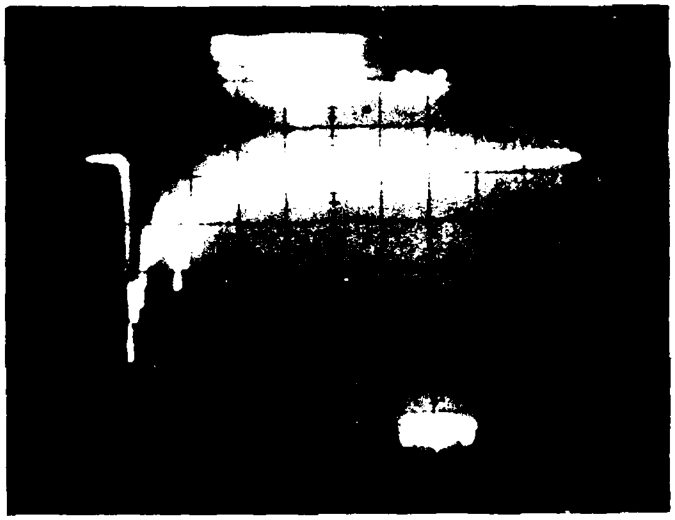

(b) Pump and first Stokes line

(c) Pump, first and second Stokes lines

Figure 14. SRS in 5.5-km length of single-mode fiber

The temporal shift (Δt) observed in the oscilloscope trace can be explained by the material dispersion (Δn) of the SiO_2 core. The observed 20 nsec shift (between the pump and S1) requires an index change of - 0.001 since,

$$\Delta n = c\Delta t/\ell \tag{9}$$

when $\ell = 5.5$ km. The refractive index of amorphous SiO_2 reported by Palik (reference 18) at 1.08 μm is n(1.08 μm) = 1.44941; while at 1.12 μm the index is n(1.12 μm) = 1.44888. The index change of Δn - 0.001 is compatible with the material dispersion observed in our experiment. We can further rule out the possibility of end reflections by assuming a typical index of 1.45 for the fiber, and the distance traversed by the reflection equal to 2ℓ. This predicts any potential reflection to occur at a temporal spacing of 50 μsec, which is several orders of magnitude larger than our observations. Therefore, we have clearly observed the amplification of the spontaneously scattered light at both S1 and S2 in our fiber laser.

5.0 FUTURE PLANS

Phase 1 of this project has ended in the generation of new wavelengths in the Raman fiber laser and the amplification of spontaneously scattered light at two wavelengths (1.117 μm and 1.18 μm). The next milestone in the development of a viable amplification system is the generation of the third through fifth Stokes lines, which should be attainable by further depletion of the pump beam (during Phase 2 of this project). This will be possible by increasing the amount of light being launched into the fiber. At this stage, increased intensity resulted in damaged fiber ends. However improved coupling and fiber end preparation should alleviate this obstacle. Further optimization of the primary pump does not seem necessary at this time, since sufficient power densities have been obtained (~ several GW/cm^2 when focused to 5 μm diameter). However, the replacement of borrowed equipment and the reoptimization of the system will require some investment in time during Phase 2. After the generation of higher order Stokes lines, advancement to amplifying a signal laser may require an optical delay. However no serious technical obstacles are anticipated. Extension to long-haul experiments can then be initiated. This will require the simultaneous launching of both the pump and signal beams into a greater than 200-km length of optical fiber.

REFERENCES

1. Russell, S.D., "Raman Scattering and Dielectric Studies of Phase Transitions in Alkali Chromates," Ph.D. Thesis, The University of Michigan, University Microfilms: Ann Arbor, MI, (1986).

2. Bloembergen, N., "The Stimulated Raman Effect," American Journal of Physics, 35, 989, (1967).

3. Wang, C.S., "Theory of Stimulated Raman Scattering," Physical Review, 182, 482 (1969).

4. Cohen, L.G., and C. Lin, "A Universal Fiber Optic (UFO) Measurement System Based on a Near-IR Raman Fiber Laser," Journal of Quantum Electronics, QE-14, 855 (1978).

5. Stolen, R.H., "Nonlinearity In Fiber Transmission," Proceedings of the IEEE, 68, 1232 (1980).

6. Stolen, R.H., "Fiber Design For Nonlinear Optics," in B. Bendow, S.S. Mitra, eds., *Physics of Fiber Optics*, Advances in Ceramics, Vol. 2, American Ceramic Society: Columbus, OH (1981).

7. Stolen, R.H., E.P. Ippen, and A.R. Tynes, "Raman Oscillation in Glass Optical Waveguides," Applied Physics Letters, 20, 62 (1972).

8. Stolen, R.H., and E.P. Ippen, "Raman Gain In Glass Optical Waveguides," Applied Physics Letters, 22, 276 (1973).

9. Lin, C., L.G. Cohen, R.H. Stolen, G.W. Tasker, and W.G. French, "Near-Infrared Sources in the 1-1.3 μm Region By Efficient Stimulated Raman Emission in Glass Fibers," Optics Communication, 20, 426 (1977).

10. J. D. Crow, "Power Handling Capability Of Glass Fiber Lightguides," Applied Optics, 13, 467 (1974).

11. Smith, R.G., "Optical Power Handling Capacity of Low-Loss Optical Fibers as Determined by Stimulated Raman and Brillouin Scattering," Applied Optics, 11, 2489 (1972).

12. Byer, R.L., "Parametric Oscillators and Non-linear Materials," in P.G. Harper, B.S. Wherrett, eds., *Nonlinear Optics*, Ch. 2, Academic Press: San Francisco, CA (1977).

13. Izrailenko, A.I., A.I. Korrigin, and P.V. Nikles, "Parametric Generation of Light in High-Efficiency Nonlinear $LiIO_3$ and α-HIO_3 Crystals," JETP Letters, 12, 331 (1970) [ZhETF Pis. Red., 12, 475 (1970)].

14. Andreev, R.B., V.D. Volosov, V.N. Krylov, "Parametric Generation Of High-Power Nanosecond Light Pulses at 0.74 - 1.85 μm," Soviet Tech. Physics Letters, 4, 105 (1978) [Pis'ma Zh. Tekh. Fiz., 4, 256 (1978)].

15. Babin, A.A., Yu.N. Belyaev, V.N. Petryakov, M.M. Sushchik, and G.I. Freidman, "Parametric Oscillator Utilizing an $LiIO_3$ Crystal Pumped by Neodymium Laser Radiation," Soviet Journal of Quantum Electronics, 6, 613 (1976) [Kvantovaya Elektron.(Moscow), 3, 1138 (1976)].

16. Lin, J.T., "Analysis of Frequency Conversion and Application of Nonlinear Crystals", *Proceedings of the International Conference LASER '86*, STS Press: McLean, VA, to be published.

17. W. Koechner, *Solid-State Laser Engineering*, Springer Series in Optical Sciences, Vol. 1, Springer-Verlag: New York, NY (1976).

18. Palik, E.D., ed., *Handbook of Optical Constants of Solids*, Academic Press: San Diego, CA (1985).

19. *Instruction Manual For Nd:YAG Laser Model 618* GTE Sylvania Laser Products Department: Mountain View, CA (n.d.).

APPENDIX A.

LASER SYSTEM OPERATING PROCEDURES

This appendix describes in detail the equipment, interconnections, and procedures used in the setup of the SRS experiment. Table A1 is a list of the major equipment used in this experiment. Table A2 describes both the electrical and water connections required by the system. This is important for future investigators since the laser system is unique. The operating procedures are then described in a menu format along with other useful documentation.

1.0 INITIAL PREPARATIONS

The initial preparations for operating this laser system included the requirement for 400 Hz, 208 V, 20 A, 3-phase power as the primary input for the laser power supply. Phase rotation must be A-B-C, wired in a "Y"-configration. Normal single phase 60 Hz, 110 V, with 40 A capacity is sufficient for all auxiliary and test equipment. The interconnections described in table A2 must be performed, followed by filling the cooling system with deionized water, and then priming the pump as per the instruction in the GTE Model 618 laser manual (reference 19). The initial optical construction relies on forming a stable cavity (according to equation 8) between the laser rod, HR and OC, and then performing the static alignment procedure outlined in reference 19.

The initiation of laser pulses requires an external trigger source for the flashlamp, which is supplied by a pulse generator (table A1 and figure 8). In anticipation of Q-switching the laser, this pulse generator also triggers the Q-switch driver (table 1 and figure 8), which subsequently sends a HV pulse to the pockels cell of the Q-switch optics. The alignment of the Q-switch optics is described in reference 19, and will not be duplicated here.

Table A1. Major component list.

ITEM	MANUFACTURER/MODEL	COMMENTS
Laser Power Supply	GTE-Sylvania/#02-1271876-1	Nd:YAG/1064 nm
Laser Transmitter	GTE-Sylvania/#02-1271876-1	PFN Electronics, External Q-switch
Laser Cooler	GTE-Sylvania/#02-1271877-1	Closed Cycle, Air/Water Heat Exchanger
Pulse Generator	California Avionics/#101AR	Output: 15 V, 100 μsec Width, 1-20 pps
Q-Switch Optics	ISOMET/#416	KD*P Pockels Cell and Polarizer
Q-Switch Driver	INRAD/#2-015	270-μsec Delay, $V_{1/4} = 5.9$ kV, w/Above Optics
Laser Mirror (HR)	PERKIN-ELMER/#582-1140	99+%R at 1064 nm, r = Infinity
Laser Mirror (OC)	PERKIN-ELMER/#582-1138	69%R at 1064 nm, AR-Coated, r = 1.47 m
Attenuator	TEKTRONIX/#011-0039-02	10x, 50 ohm, 2 W
Joulemeter Detector	GENTEC/#PRJ-D	1.91 V/J Calibrated Head #ED 500
Ge Pin Diode Detector	Antel Optronics/#AR-G10	25-mA/mV Responsivity w/#PS-G10 Power Supply
Spectometer	Jarrell Ash/#82-020	590 Grooves/mm
Oscilloscope	Tektronix/#7104	w/#7A26 Dual Trace Amp & #7B15 Delaying Time Base
Alignment Laser	Hughes Aircraft/#4020	HeNe/632.8 nm Wave-length 10 mW Max.

Table A2. System interconnections.

ELECTRICAL CONNECTIONS:

FROM	TO
J1 Laser Power Supply (LPS)	400 Hz,208 V,3 ϕ,20 A Power Line
J2 LPS	J3 Laser Transmitter (LT)
J3 LPS	J1 LT
J4 LPS	J2 LT
J5 LPS	J1 Laser Cooler
J7 LPS	<Output> Pulse Generator
Rear Panel Pulse Generator	60 Hz,110 V,1 ϕ Power Line
<Output> Pulse Generator	<Input> 10x Attenuator
<Output> 10x Attenuator	<Trigger Input> Q-switc Driver
Rear Panel Q-switch Driver	60 Hz, 110 V, 1 ϕ Power Line
HV Q-switch driver	Male BNC Pockels Cell
Flashlamp Anode (Front of Laser Head)	Vacuum Relay inside transmitter
Flashlamp Cathode (Rear of Laser Head)	Insulating spacer inside transmitter

COOLING LINE CONNECTIONS:

FROM	TO
OUT Laser Cooler	Either port of laser head
Either Port of Laser Head	Either Port on PFN inside transmitter
Either Port of PFN Inside Transmitter	IN Laser Cooler

2.0 LASER START-UP PROCEDURE

1. Set-up system as described in previous paragraphs and tables A1 and A2.

2. Verify that the front-panel voltage adjust on the laser power supply (LPS) is fully counter-clockwise for minimum operating voltage, and front panel LPS breaker switch is in the off position (down).

3. Turn the front panel breaker switch on the LPS to the ON position (up) to start the cooling system. Observe that the power-on and interlock open lamps on the LPS are illuminated. It is recommended that approximately 2 minutes are allowed for the thyratron tube in the transmitter to warm up before further operation. During this time, routine inspection of cooling lines for leaks or damage is recommended. This laser does not (unlike Model 618) have a deionizer lamp to indicate if the closed cycle cooling water is contaminated. The electrical conductivity of contaminated water may quench the HV flashlamp start and simmer pulses preventing laser operation. If this occurs, it requires the replacement of the water and deionizing filter cartridge in the laser cooler. The appropriate procedure is described in reference 19.

4. Turn the key switch to the ON position, the interlock lamp will extinguish.

5. Depress the black HV-ON pushbutton. Observe that the HV-ON and simmer lamps are illuminated. This initiates the simmer current on the flashlamp and charges the PFN capacitor. Note: A high frequency audio signal from the power supply is present during normal operation.

6. Turn on the pulse generator, set output pulse amplitude to 15 V, pulsewidth of 100 μsec and period between 0.05 and 1.00 seconds (corresponding to a range of 1 to 20 pulses per second). Depress the white initialize button on the pulse generator to start the trigger pulse and begin laser output.

7. Increase the setting of the voltage adjust on the LPS to obtain the desired power output.

8. For Q-switch operation, turn on power to Q-switch driver and set delay to 270 μsec by turning the thumbwheel dials. Set the quarter-wave high voltage ($V_{1/4}$) using the thumbwheel dial (for the Isomet KD^*P crystal: $V_{1/4}$ = 5.9kV). If Q-switch output does not result, adjustment of the rear panel output level knob of the Q-switch driver will be necessary. [See figure A1 for the flashlamp and Q-switch timing diagram.]

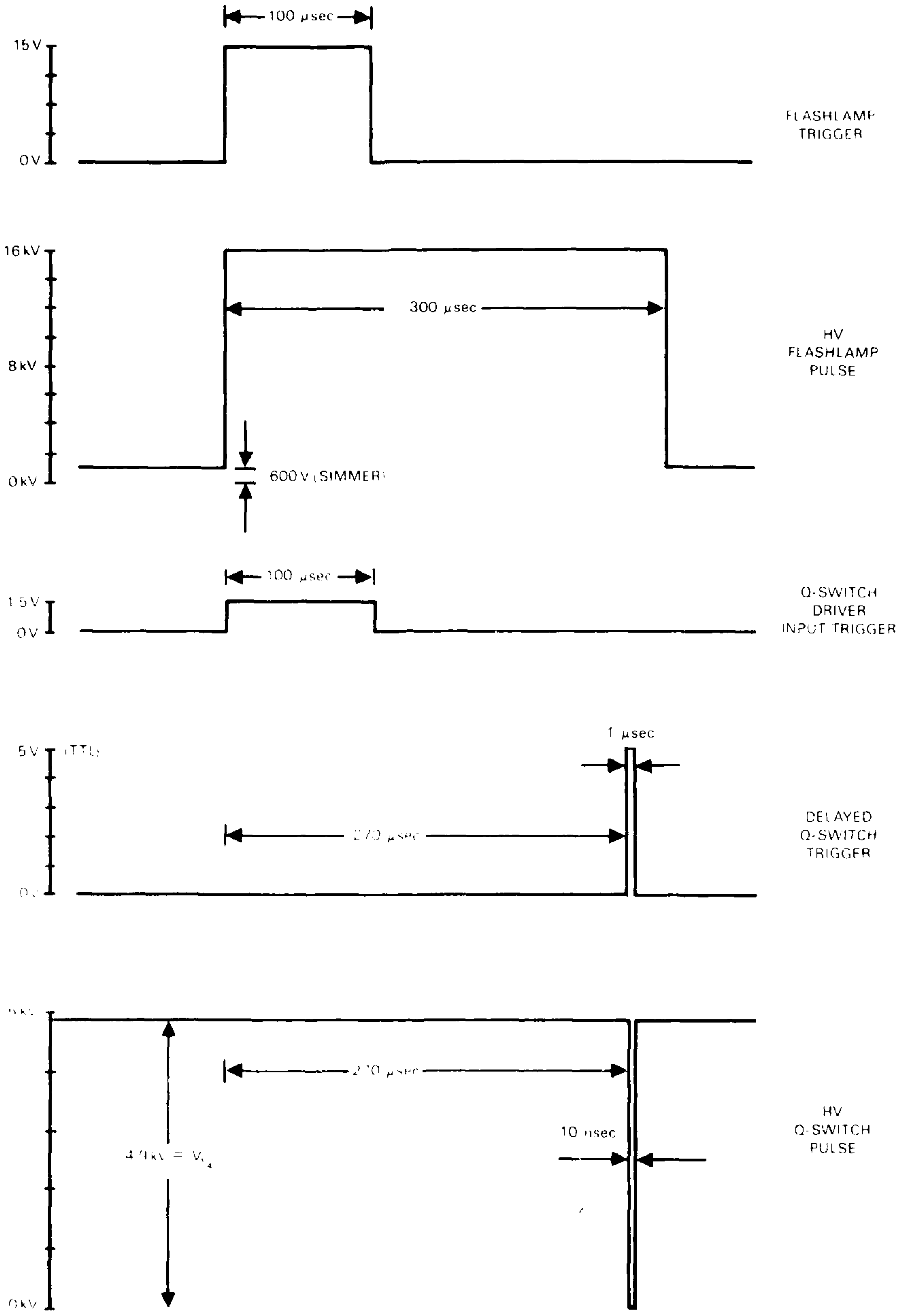

Figure A1. Timing diagram

3.0 LASER SHUT-DOWN PROCEDURE

1. Turn down HV to Q-switch optics using thumbwheel dial.

2. Turn voltage adjust on LPS fully counter-clockwise for minimum operating voltage.

3. Turn off HV to laser by depressing red-HV-OFF button on front panel of LPS.

4. Allow a few minutes for the laser rod to cool, while doing so turn off power to pulse generator, Q-switch driver and test equipment in use.

5. Turn off laser cooling by returning the front panel breaker switch to the off (down) position. The HV should always be off prior to operating the breaker switch.

6. Turn the key switch off.

4.0 ADDITIONAL COMMENTS

Any attempts to operate the laser beyond its power capability will result in a breaker button on the front panel of the LPS disengaging, resulting in a stoppage of laser output. This is remedied by turning down the voltage adjust to its minimum value (fully counter-clockwise), depressing the HV off button, thus depressing the breaker button, and thereby resetting the laser for operation. Resumption of laser action can be obtained by depressing the HV ON button in conjunction with a setting appropriate value of the voltage adjust.

APPENDIX B.

COMPONENT PURCHASE LIST

NOTE: This appendix lists the major purchases funded by the IED Project during the first half of FY 87. Incidental purchases, such as the film for the oscilloscope camera obtained direct from NOSC Supply, are not included in table B1 below.

Table B1. List of purchased components.

Stub#/Date	Source	Item	Model #	Qty	Unit Price	Price	Rec'd
1) HPN-00-87 12/86	Newport Corp.	a) Precision Fiber Coupler	F-915	1	$520.	520.	2/87
		b) Optical Rail	URL-18	1	95.	95.	"
		c) Diode Laser focusing lens	F-L10	1	120.	120.	"
		d) Mirror Mount	MM-2	2	48.	96.	"
		e) Beamsplitter Mount	MM2-1A	1	61.	61.	"
2) FPH-33-87 12/86	Melles Groit	a) Laser Mirror 99.5%R	08MLQ003/326	1	159.	159.	1/87
		b) Laser Mirror 99.5%R @ 45°	08MLQ003/436	2	159.	318.	"
		c) Laser Output Coupler 80%R	08C0B028	1	235.	235.	"
		d) Laser Output Coupler 70%R	08C0B027	1	235.	235.	"
3) FPH-32-87 1/87	Oriel Corp.	a) Heat Transmitting Mirror	57430	2	193.	386.	2/87
		b) Fused Silica Lens	39312	2	118.	236.	"
		c) Dispersing Prism	46090	1	356.	356.	"
4) FPH-25-87 1/87	Newport Corp.	a) Adj Radius Chucks	AC-1	6	64.	384.	2/87
		b) Standard Base	B-2	8	20.	160.	"
		c) Post Holders	MPH-2	6	18.	108.	"
		d) Post Holders	MPH-1	2	16.	32.	"
		e) Posts	MSP-1.5	8	4.	72.	"
		f) Var Lens Holder	VLH-3	2	70.	140.	"
		g) Posts	MSP-1	2	8.	16.	"
5) FPH-39-87 1/87	Research Devices	IR-Microscope Objective	#0012	2	350.	700.	2/87

Table B1. List of purchased components (cont'd).

Stub#/Date	Source	Item	Model #	Qty	Unit Price	Price	Rec'd
6) FPH-68-87 2/87	ILC Technology	Flashlamp	#L2006	3	250.	700.	4/87
7) FPH-69-87 1/87	Newport Corp.	a) IR Sensor Card	F-IRC1	1	31.	31.	2/87
		b) Diode Laser Objective Lens	F-L10B	2	115.	230.	"
		c) Cable Clamp	F-CC	4	42.	168.	"
		d) Collar	MPC	5	5.	25.	"
		e) Post	MSP-2	3	10.	30.	"
		f) Post	MSP-1	2	8.	16.	"
		g) Base	B-2	4	21.	84.	"
		h) Postholder	MPH-2	7	18.	126.	"
		i) Post	SP-2	4	10.	40.	"
		j) Post	MSP-1.5	2	9.	18.	"
		k) Mirror Mount	MM2-1A	4	62.	248.	"
		l) Post	SP-3	4	11.	44.	"
8) FPH-81-87 2/87	CVI Laser Corp.	70%R Laser Mirror	PR10-70-1.0	1	360.	360.	3/87
		99%R Laser	Y1-10-0	1	275.	275.	"
9) HTN-03-07 2/87	Philips Test & Measurement	Pulse Generator	PM5705	1	674.	674.	2/87
10)HTN-04-87 2/87	Inter-active Radiation Inc.	Electro-optic Q-switch	202-090	1	1430.	1430.	4/87
		Q-switch Driver	2-015	1	1675.	1675.	"
		Gimbal Mount	875-430	1	405.	405.	"

TOTAL COST: $11K (approximately, for first-half FY 87 equipment expenditures).

APPENDIX C

FIBER SPECIFICATIONS

The 5.5-km fiber used in these experiments is a continuous, unspliced single mode fiber purchased from Corning Glass Works in 1981 by Drs. C.T. Chang and H.E. Rast, Code 562, NOSC, San Diego, CA. Table C1 below shows the optical parameters specified by P.E. Blaszyk of Corning. The fiber has a coating of Corning CPC™ acrylate composite for strength preservation, and was supplied on a standard Corning measurement drum suitable for optical measurements. Corning recommends chemical removal of the coating with methyl chloride, although mechanical stripping may be used with the possible risk of fiber strength degradation. The fiber was made using the proprietary Corning MCVD process.

Table C1. Optical parameters of 5.5 km length fiber.

Attenuation at:	850 nm	=	2.29 dB/km
	900 nm	=	2.02 dB/km
	950 nm	=	5.59 dB/km
	1060 nm	=	1.39 dB/km
	1150 nm	=	2.23 dB/km
	1200 nm	=	4.29 dB/km

Cutoff Wavelength	700 nm
Core Diameter	5.6 μm
Δ (index difference)	0.004
Glass OD	110.0 μm
Proof Test	25 Kpsi
Coating Diameter	250 μm

Figure C1 shows the attenuation spectra measured by Corning between 600 nm and 1590 nm for this fiber. Measurements beyond 1200 nm were attributed to noise. Figure C2 shows a refracted near-field scan and microphotograph of one end of the fiber. The core is circular and concentrically located within the fiber, with an index difference between the core and cladding (Δ) of 0.004.

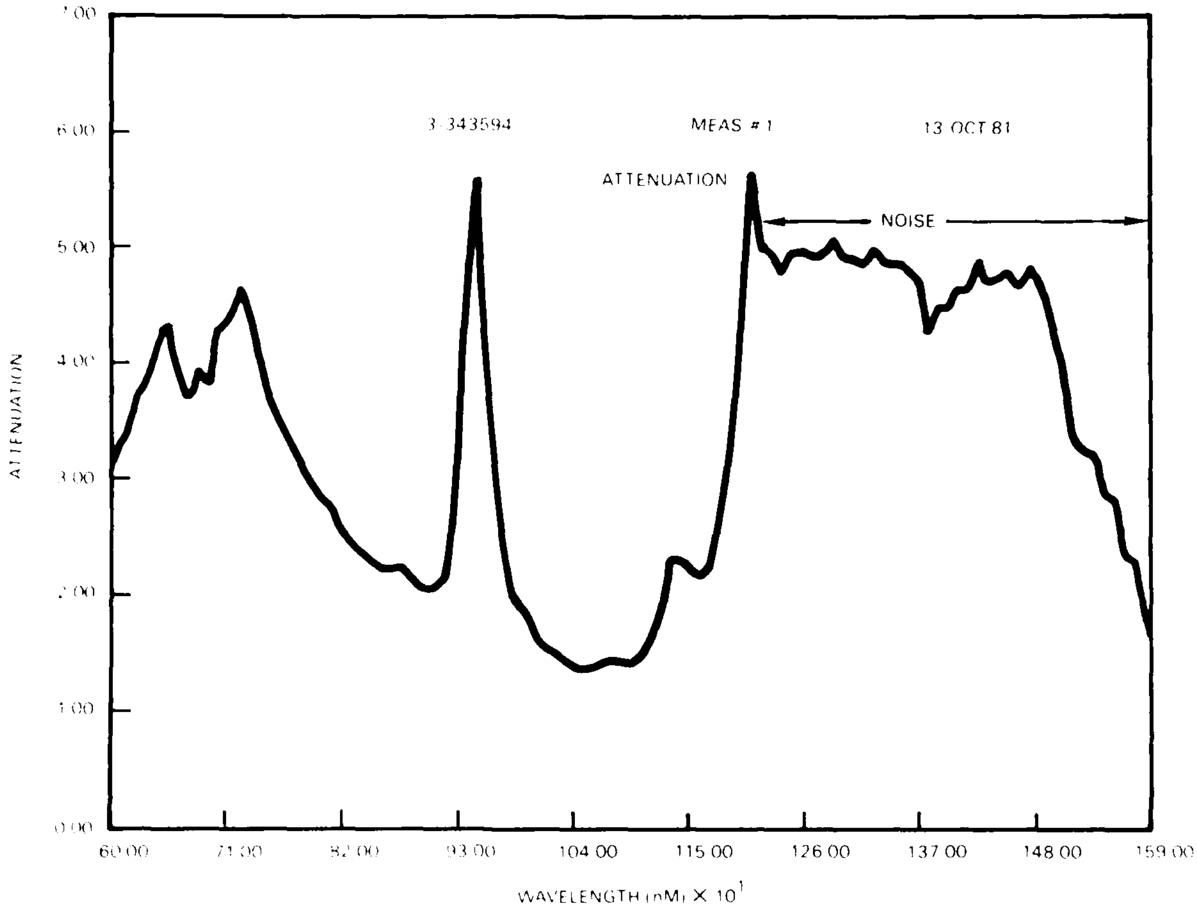

Figure C1. Attenuation spectrum of 5.5-km length of single-mode fiber.

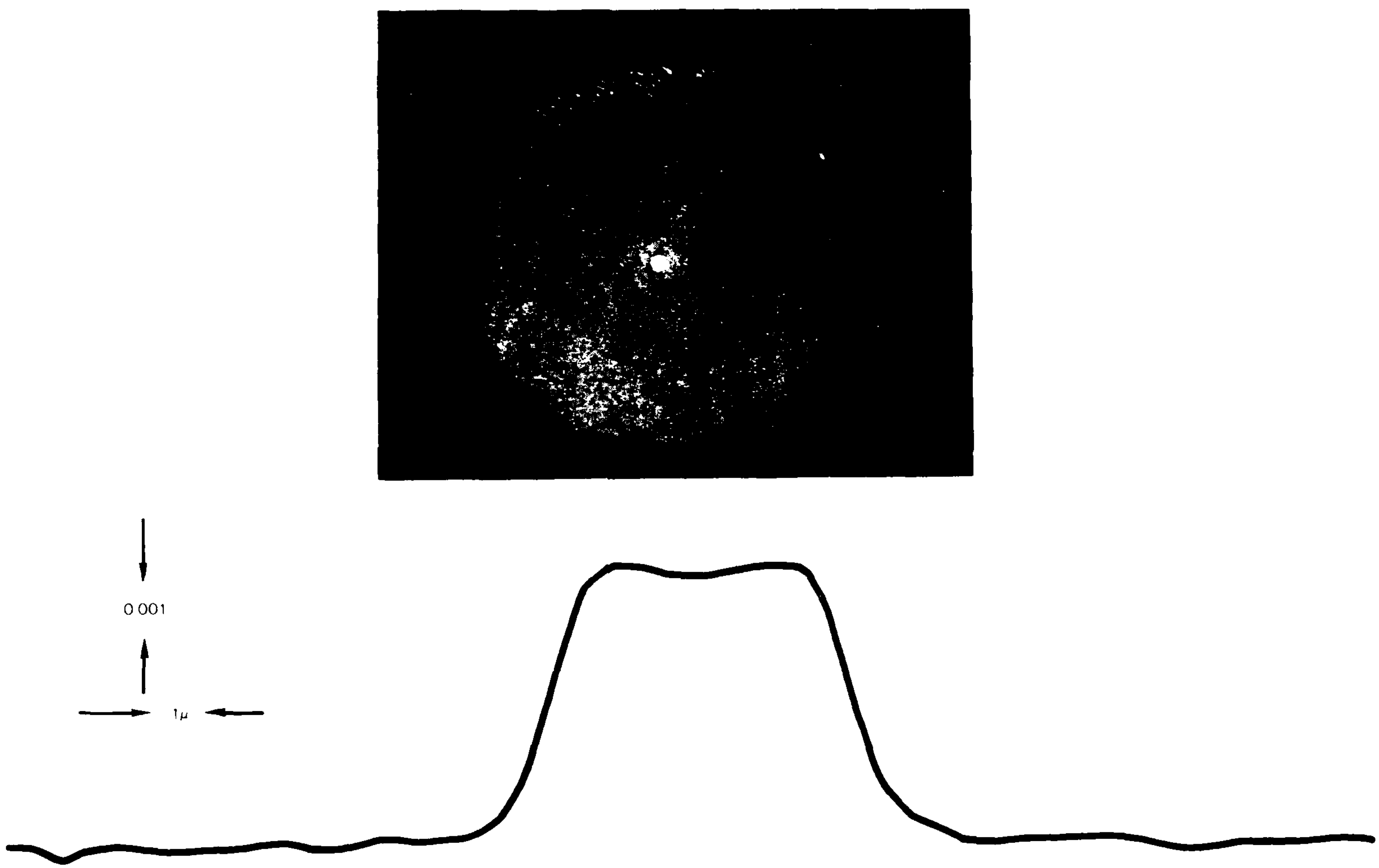

Figure C2 Micrograph and refracted near-field scan of end of 5.5-km fiber.

DATE

FILMED

4 8